Journal of Nuclear Materials 452 (2014) 235–240

Contents lists available at ScienceDirect

Journal of Nuclear Materials

journal homepage: www.elsevier.com/locate/jnucmat

Effects of thermal aging on microstructure and hardness of stainless steel weld-overlay claddings of nuclear reactor pressure vessels

T. Takeuchi [a,*], Y. Kakubo [b], Y. Matsukawa [b], Y. Nozawa [b], T. Toyama [b], Y. Nagai [b], Y. Nishiyama [c], J. Katsuyama [c], Y. Yamaguchi [c], K. Onizawa [c], M. Suzuki [a]

[a] Japan Atomic Energy Agency, Oarai, Ibaraki 311-1393, Japan
[b] The Oarai Center, Institute for Materials Research, Tohoku University, Oarai, Ibaraki 311-1313, Japan
[c] Japan Atomic Energy Agency, Tokai, Ibaraki 319-1195, Japan

ARTICLE INFO

Article history:
Received 11 June 2013
Accepted 4 April 2014
Available online 17 May 2014

ABSTRACT

The effects of thermal aging of stainless steel weld-overlay claddings of nuclear reactor pressure vessels on the microstructure and hardness of the claddings were investigated using atom probe tomography and nanoindentation testing. The claddings were aged at 400 °C for periods of 100–10,000 h. The fluctuation in Cr concentration in the δ-ferrite phase, which was caused by spinodal decomposition, progressed rapidly after aging for 100 h, and gradually for aging durations greater than 1000 h. On the other hand, NiSiMn clusters, initially formed after aging for less than 1000 h, had the highest number density after aging for 2000 h, and coarsened after aging for 10,000 h. The hardness of the δ-ferrite phase also increased rapidly for short period of aging, and saturated after aging for longer than 1000 h. This trend was similar to the observed Cr fluctuation concentration, but different from the trend seen in the formation of the NiSiMn clusters. These results strongly suggest that the primary factor responsible for the hardening of the δ-ferrite phase owing to thermal aging is Cr spinodal decomposition.

1. Introduction

Weld overlay claddings made of stainless steel are used on the inner surfaces of commercial water-cooled reactor pressure vessels (RPVs) as protective barriers against corrosion. These claddings are subjected to both neutron irradiation and prolonged thermal aging at a service temperature of about 300 °C. The thermal and irradiation environments may cause microstructural changes in the claddings, resulting in the degradation of their mechanical properties and corrosion behavior. Thus, a detailed analysis of the microstructural evolution of these claddings is necessary for ensuring the integrity of RPVs.

The claddings are of the duplex type, consisting of two phases. It is composed of approximately 90% austenite and 10% δ-ferrite having net-like structures [1]. The presence of the δ-ferrite and austenitic phases is responsible for the claddings exhibiting enhanced corrosion resistance [2]. However, it is known that the δ-ferrite phase undergoes significant hardening during thermal aging, resulting in an increase in its ductile-brittle transition temperature (DBTT), and a decrease in its upper shelf energy [3–5].

In duplex stainless steels, fluctuations in the Cr concentration owing to spinodal decomposition and the formation of a G phase are considered to play a key role in the hardening of the δ-ferrite phase [6,7]. We had previously investigated the microstructural changes in claddings aged at 400 °C for 10,000 h via three-dimensional atom probe tomography (APT) [8,9]. In the as-received materials subjected to post-welding heat treatment (PWHT) with subsequent furnace cooling, a slight fluctuation of the Cr concentration was observed due to spinodal decomposition in the δ-ferrite phase, but not in the austenitic phase. The thermal aging caused not only an increase in the degree of spinodal decomposition, but also the precipitation of G phases in the δ-ferrite phase with the composition ratio Ni/Si/Mn being 16:7:6.

Danoix et al. [10] have found that, in the case of cast duplex stainless steels, the hardening at the δ-ferrite phase in fully annealed samples is associated with spinodal decomposition but not with G-phase precipitation. On the other hand, Yamada et al. [11] found that the G phase significantly contributed to the hardening in similar annealing recovery tests. Hence, the effect that the G phase has on hardening is still not clear.

In the case of the claddings, the effects of the duration of aging on the microstructure and the relationship between the microstructure and the hardness of the claddings have not yet been determined because an accurate estimation of the hardness of

* Corresponding author. Tel.: +81 29 266 7032; fax: +81 29 266 7071.
E-mail address: takeuchi.tomoaki@jaea.go.jp (T. Takeuchi).

http://dx.doi.org/10.1016/j.jnucmat.2014.04.003
0022-3115/

Table 1
Chemical composition of the claddings.

	C	Si	Mn	P	S	Ni	Cr
wt.%	0.022	0.530	1.34	0.010	0.005	11.79	22.34
at.%	0.102	1.054	1.36	0.018	0.009	11.22	23.99

the δ-ferrite phase has not yet been achieved, since the δ-ferrite phase is typically less than 5 μm in width.

The objective of this study was to investigate the effect of thermal aging on the microstructure and hardness of claddings subjected to thermal aging at 400 °C for periods of 100–10,000 h, using APT and nanoindentation testing, to determine the mechanism responsible for the hardening of the claddings.

2. Experimental

The claddings used were fabricated using the electroslag weld overlay method. The chemical composition of the claddings is listed in Table 1. The as-welded sample was subjected to a PWHT at 615 °C for 7 h and subsequent furnace cooling (this sample is referred to as the as-received sample). This sample consisted of approximately 8% δ-ferrite having net-like structures in an austenite matrix. The width of the δ-ferrite phase was a few micrometers. Cladding samples were then thermally aged at 400 °C for 100, 1000, 2000, and 10,000 h, respectively. The samples for the APT were first lifted via the lift-out method using a dual-beam focused ion beam/scanning electron microscopy (FIB/SEM) ion milling system [12]. They were then sharpened and either the austenite phase or the δ-ferrite phase was selected at the tips of the needle-like specimens. In order to analyze gallium-free specimens, the damage caused by gallium implantation during fabrication via FIB was minimized by using low-energy ions in the final process. Only the gallium-free regions were used for the analyses.

An ultraviolet laser-pulse APT system (Cameca Instruments LEAP 4000X-HR) equipped with an energy-compensating reflection lens [13–15] was used to analyze the microstructures. The measurements were performed at a laser pulse energy of 60 pJ and a repetition rate of 200 kHz at approximately 60 K. A high direct current bias in the range of 3–10 kV was typically used. Approximately a few tens of millions of atoms were typically collected during each measurement.

The surfaces of the samples for the nanoindentation tests were treated using the following procedure. The samples were mounted on an epoxy resin base, and were then mechanically polished with sandpaper, followed by electrochemical polish at 8 °C in an ethanol solution containing 5% perchloric acid. Finally, they were chemically polished using nitro-hydrochloric acid (aqua regia).

The nanoindentation tests to determine the hardness were performed using a nanoindenter (ENT-1100a, Elionix Inc.). Since the width of the net-like δ-ferrite phase was only a few micrometers as mentioned above, the size of the indentations needed to be less than a few hundreds of nanometers so that they were not influenced by the surrounding austenite phase. However, if the indentations were too shallow, they would be affected by the surfaces of the samples. Thus, in order to determine the optimal indentation load, we used loads of 1, 2, 3, 5, and 7 mN and observed the indents formed using SEM. The nanoindentation hardness of the cladding material with indentation load and the SEM images of the indentations are shown in Fig. 1(a) and (b), respectively. The indentation depth with 1 mN, where the SEM image of the indentation is no longer clear, was estimated less than 100 nm where surface effects could exist. On the other hand, the measurement values with more than 3 mN, which partly include the hardness of austenite, scatter and the distributions tend to shift toward lower range with the load. On the basis of these results, an indentation load of 2 mN was used in this study.

3. Results

3.1. APT observation

Three-dimensional maps showing the elemental concentrations of Fe, Cr, Ni, Mn, and Si in the δ-ferrite phases of the as-received samples as well as those thermally aged at 400 °C for 100–10,000 h are shown in Fig. 2. These elemental maps were constructed using 20-nm-thick slices to clearly illustrate in detail

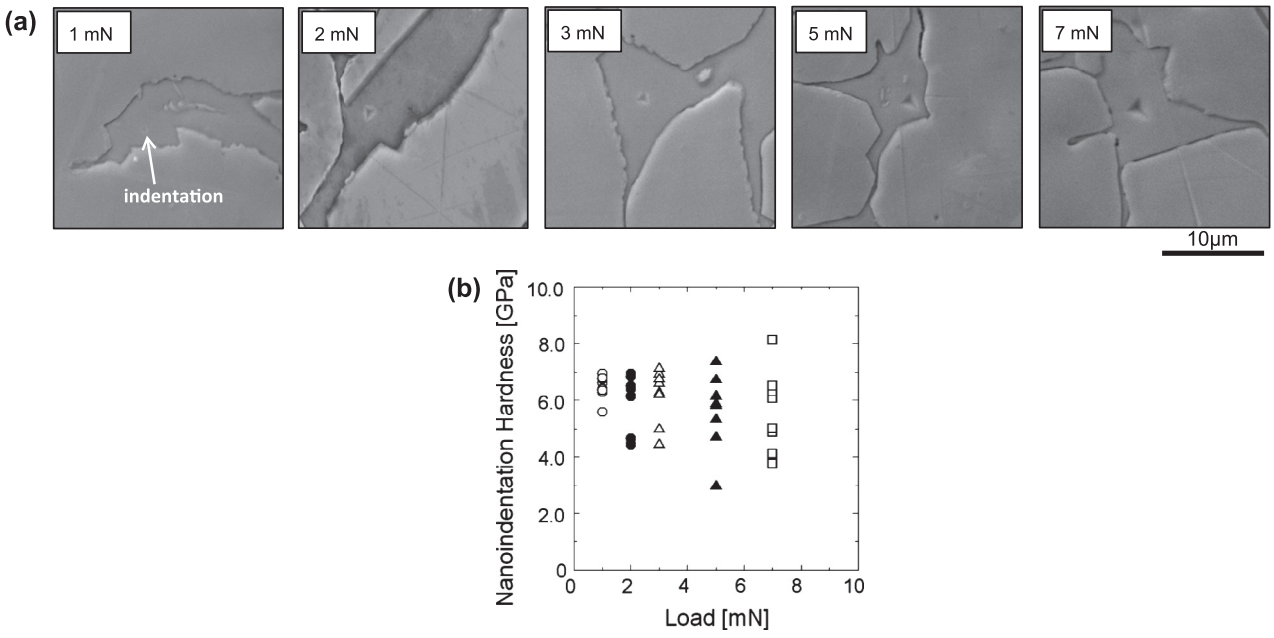

Fig. 1. (a) SEM images of indentations made with loads of 1 mN, 2 mN, 3 mN, 5 mN, and 7 mN, and (b) the nanoindentation hardness at the δ-ferrite phase of the trial cladding material with indentation load.